Chlorophyll Changes Using Neural Network and Vegetation Indices in Tropical deciduous forest

Saurabh Kumar Gupta
Central University of Jharkhand
Arvind Chandra Pandey (arvindchandrap@yahoo.com)
Central University of Jharkhand

Research

Keywords: Leaf Chlorophyll content, Forest Health, Plant Stress, Radiative transfer model, Vegetation Indices

Posted Date: April 27th, 2020

DOI: https://doi.org/10.21203/rs.3.rs-23278/v1

Abstract

Background: Ongoing climate and Earth's atmosphere changes create profound effect on distribution and composition of forest, as well as on the fauna that depends on forest. The Sentinel-2A satellite data eases the mapping of Leaf Chlorophyll Content (LCC) at higher spatial and temporal resolution. In the present study, the temporal dimension of LCC was evaluated as an indicator of plant stress. LCC was retrieved using the inversion of the radiative transfer model based on an artificial neural network. The data used for Spatio-temporal modelling of LCC was Landsat data.

Result: From the Sentinel imagery derived vegetation indices, it was found that the narrowband indices having high correlation with LCC were pigment specific simple ratio and normalized difference index (45) ($R^2 > 0.7$; $p < 0.001$) centred at 665 nm, 705 nm, and 740 nm. Landsat 8 infrared percentage vegetation index had a strong relationship with LCC (R^2 =0.8). The Spatio-temporal (1997 to 2017) plant stress were detected using changes in LCC through an equation of correlation. The negative changes and deterioration of LCC were seen in the forest during the year 1997 to 20I7(rate = -1.2 $\mu g cm^{-2} year^{-1}$) showing higher rate of forest health decline.

Conclusion: The 33% of plant stress increased currently in the protected forest mainly because of anthropogenic influences. These vast decline in the chlorophyll gives rise to various photosynthetic vulnerabilities in forest ecosystem and indirectly affects human including wildlife.

1. Introduction

Forests worldwide are becoming susceptible to an increasing size of abiotic and biotic disturbances [1–4]. The forest makes up high productive plants and resembles a significant carbon sink on the planet, which entails understanding of their spatiotemporal changes utmost important [5–6]. Forests are prone to degradation largely because of anthropogenic disturbances as well as climate changes [7–8]. With coupling with GIS, remote sensing technology proved to be a powerful tool for forest analysis [9].

The simulating forest photosynthetic activity is crucial to define tropical environmental controls and ecosystem metabolism [10–11, 6]. Chlorophyll is a natural green particle in plant cells and plays a crucial part in the photosynthesis process. There are two classes of chlorophyll in plants, chlorophyll a and b which function as a photoreceptor in photosynthesis. The deficiency of these two chlorophyll contents may result in an unhealthy forest. Low chlorophyll content can limit primary production and hence, photosynthetic potential [12]. Chlorophyll is an indicator of physiological status, senescence, and stress [13–14]. The forest health condition changes need the understanding of chlorophyll content changes. Yang et al. 2017 [15] worked on the temperate forest by showing the seasonal variation of chlorophyll on ground based Normalized Difference Vegetation Index (NDVI) imagery. Pastor-Guzman et al.,2015 [16] performed on spatiotemporal mapping of chlorophyll in the Mangrove forest by using Landsat derived NDVI- Green. Zarco-Tejada et al.,2018 [17] analysed the temporal changes of red edge spectra, which is

sensitive to chlorophyll for estimating canopy defoliation and pigment degradation. Croft et al., 2014 [18] analysed growing season temporal variation of leaf chlorophyll content in a temperate deciduous forest.

Satellite remote sensing has difficulties in the estimation of chlorophyll beneath the canopy. Top of canopy reflectance is empirically related to chlorophyll concentration in the forest [19, 15]. This principle applied to create radiative transfer models based on the artificial neural network for estimating chlorophyll concentration. The original inspiration of this technique comes from the working of the central nervous system and with coordination of the neurons (and their dendrites, axons, and synapses), which make up significant information processing systems. In a neural network model, nodes ("neurons," units" or "processing elements") are coming together to make a network of nodes, therefore called "neural network. For operational applications, the inversion techniques are applied, which is based on a pre-trained reflectance database. The model so develop is a mixture of PROSPECTS [20] and SAIL [21] called PROSAIL to see biophysical properties of the forest.

Remote sensing-based appraisal of biophysical characteristics of the forest is often getting through developing empirical relationships between field-measured vegetation properties and vegetation indices [18]. While using the PROSAIL model and satellite-determined vegetation indices to evaluate the chlorophyll content of the leaf in different vegetation types, only few of studies focused on sub-tropical forest [22–23]. Given the significance of foliar pigments as surrogates of forest physiological status, phenology, health condition, and the gross primary productivity, it is crucial to evaluate the exactness of vegetation indices to foresee LCC.

Forest in the study area is affected by fragmentation [24] and connectivity weakening [25]. The forest of Jharkhand comprised 29% of its total geographical area, and it is prone to degradation due to many natural and anthropogenic factors including forest fire hazard and drought, which lead to loss of green cover [26]. This study examines the usefulness of sentinel 2A imagery for retrieving leaf chlorophyll content in the forest. Our primary aim is to prove that the multispectral sensor Landsat 8 able to create maps of spatiotemporal variation of leaf chlorophyll focus in the sub-tropical forest. Change detection of chlorophyll content using combination of Sentinel 2A and Landsat is new in the research.

2. Data Used And Methodology

2.1. Study Area

Hazaribagh wildlife sanctuary in Jharkhand (India) is situated covers an area of 186 km^2(Fig. 1). It lies between 24°45'22" N to 24°08'20"N latitude and 85° 30'13" E to 85°21'58"E longitude. The place is home to Peafowl, Nilgai Sambar, Chital, Sloth bears, Black bears, Hyena, and Pigeons. The area experiences subtropical and humid monsoon climate characterized by hot summers (40°C) and mild winters (4°C).

2.2. Data collection

The field study allowed us to find which forest cover types had what amount of leaf chlorophyll content. The numerous portions of the study area transformed into open and scrub forest from dense forest (Fig. 2). The present study used Sentinel 2A data for retrieving LCC and Landsat data for Spatio temporal mapping of LCC (http://earthexplorer.usgs.gov) (Table 1).

Table 1
Satellite data used in the present study

Sensor	Date gained	Path/row	Sun Height
20160213T101928_A003362_T45QUG (Sentinel 2 A)	2016-02-13	140/43	-
LT51400431997319SGI00	1997-11-15	140/43	40.20
LT51400432000312BKT00	2000-11-07	140/43	42.68
LT51400432005309BKT01	2000-11-07	140/43	44.38
LT51400432008334KHC01	2008-11-08	140/43	43.45
LC81400432013315LGN02	2013-11-11	140/43	44.19
LC81400432017310LGN00	2017-11-06	140/43	45.38

2.3. Data pre-processing

2.3.1. For Landsat data

Raw satellite data required atmospheric correction for retrieving actual reflectance of objects. For this purpose, the data was automatically corrected using SAGA GIS module and to surface reflectance by Dark Object Subtraction (DOS) method. The (DOS) method presumes that over satellite image there are present features having near-zero percent reflectance (i.e., water and shadow) and this must be removed. It is calculated by below Eq. (1): (see Equation 1 in the Supplementary Files)

Where, $p\rho$ is the DOS corrected image and $Cos\left(\emptyset_z\right)$ is the cosine form of solar zenith angle and E_0 is the exoatmospheric solar spectral irradiance.

The Radiance (L_λ) was calculated through the below-given equation (Eq. 2)

L_λ = Bias + (Gain* DN) (2)

Where DN = Digital Number and the relflectance (P_λ) was computed by given below equation (Landsat Science User Data Handbook) (Eq. 3).

$P_\lambda = \pi * L_\lambda * d^2 / ESUN_\lambda * Cos\theta$ (3)

Where P and L are reflectance respectively and at-satellite spectral radiance, ESUN is mean solar exoatmospheric irradiances for a band, d is the Earth-Sun distance, and cos ø is the solar incidence angle.

2.3.2. For Sentinel 2 A data

The sentinel 2A undergoes various stages of atmospheric correction using SNAP software. The Sent2core plugin was used for transformation of Sentinel level 1 image to level 2 resembles conversion of digital number of images to surface reflectance. It helps to correct images from the presence of aerosol, ozone level distortion, type of locality, mid-latitude abnormality and topographical variations. The IdePix Sentinel MSI plugin was used for masking of land/water/ cloud in the imagery.

2.4. Computing chlorophyll content

The method of inversion of PROSAIL using SNAP software(step.esa.int/main/toolboxes/snap) is given in Fig. 3 and its illustration below.

The inputs (Sentinel2 surface reflectance 8 bands B3, B4, B5, B6, B7, B8a, B11, B12) and geometry, cos (Viewing_Zenith), cos (Sun_Zenith), cos (relative_azimuth_angle) and output (LCC) values were firstly normalized according to Eq. 4.

$X^* = 2*(X-XMin)/(XMax-XMin)-1$ (4)

Where X^* is the normalized input, X the original value, Xmin and Xmax respectively the minimum and maximum values.

Every artificial neural networking has the hidden layer and the output layer. The layer outlined by its number of neurons, which has biases, weight, and transfer function which is developed earlier and embedded in PROSAIL model.

The neurons have transfer function called tangent sigmoid transfer function (Eq. 5);

$Y = Tansig(x) = 2/(1 + \exp(-2x))-1$ (5)

While an output layer with the transfer function is linear (y = x). It is simply involving the application of reverse function used to enter normalization given in Eq. 6.

$Y = 0.5 (Y^*+1) * (Ymax-Ymin) + Ymin$ (6)

where Y^* is normalized output value (LCC) issuance from neural network, and Ymin and Ymax were calculated over the neural network training dataset.

The accuracy assessment of LCC is given in Fig. 4. It shown good Root-mean-square Deviation (RMSE) of 56.29 μg cm^{-2}. In case of LCC, significant correlation coefficient of 0.87 seen using artificial neural networking [28].

2.4. Vegetation indices

A vast number of vegetation indices have been used and evaluated for measuring plant physiological conditions using simulated and empirical data [29]. 9 vegetation indices were calculated using the Sentinel 2A and Landsat 8 OLI data sets, from which 7 were broadband indices while 2 vegetation indices were narrow-band indices (Table 2). The chlorophyll concentration is well predicted in the wavelengths between 400 nm to 725 nm with multiple scattering in the Near Infrared (NIR) region. Therefore, vegetation indices covered these ranges are useful in modelling LCC [39]. The wavelength of broadband vegetation indices was: Blue (436–528), Red (625–691), Green (512–620), and NIR (829–900 nm). The broad band vegetation indices were calculated using the Landsat 8 OLI. Both Broadband and narrowband indices were used to measure the relationship between LCC and the spectral response function of the forest leaf. Theoretical analyses and field studies have shown that vegetation indices are near-linearly connected to estimate biophysical variables [40]. In the present study, indices were taken because most of the biophysical measurements, for example chlorophyll estimation using remote sensing depend upon the spectral proprieties of vegetation by a semi-empirical linkage with vegetation index [41, 42]. In other means the spectral vegetation indices are popularized for retrieving chlorophyll content from reflectance factors.

Table 2
Vegetation indices used in the study

VI	*Formula*	*Reference*
Infrared Percentage Vegetation Index (IPVI)	$\frac{\mathrm{NIR}}{\mathrm{NIR}+\mathrm{RED}}$	[30]
Green Vegetation Index (GVI)	(-0.2848 * TM_1) + (-0.2435*TM_2) + (-0.5436*TM_3) + (0.7243* TM_4) + (0.0840*TM_5) + (-0.1800*TM_7)	[31]
Global Environmental Monitoring Index (GEMI)	$\mathbf{eta}(1-0.25*\mathbf{eta})-\frac{\mathbf{Red}-0.125}{1-\mathbf{Red}}$ *Where*: $\frac{2\left(\mathrm{NIR}^2-\mathrm{Red}^2\right)+1.5*\mathrm{NIR}+0.5*\mathrm{RED}}{\mathrm{NIR}+\mathrm{RED}+0.5}$	[32]
Green Atmospherically Resistance Index (GARI)	$\frac{\mathrm{NIR}-[\mathrm{Green}-\gamma(\mathrm{Blue}-\mathrm{Red})]}{\mathrm{NIR}+\mathrm{Green}-\gamma(\mathrm{Blue}-\mathrm{Red})}$	[33]
Difference Vegetation Index (DVI)	NIR-RED	[34]
Atmospherically Resistance Vegetation Index (ARVI)	$\frac{\rho_{800}-[\rho_{680}-\gamma\left(\rho_{450}-\rho_{680}\right)]}{\rho_{800}+[\rho_{680}-\gamma\left(\rho_{450}-\rho_{680}\right)]}$	[35]
Ratio Vegetation Index (RVI)	*NIR/RED*	[36]
Pigment Specific Simple Ratio (PSSRA)	*Band 7/ Band 4 (Sentinel)*	[37]
Normalized difference Index (ND45)	*(Band5-Band4)/(Band5 + Band4)* Where band 5 and 4 are sentinel 2A bands	[38]

2.5. Modelling change detection

The forest health and stress were examined by LCC value, its decrease in value shows forest health decline and increment in plant stress. The Spatio-temporal changes of chlorophyll were computed using a grid statistics algorithm in SAGA GIS. Then, the scatter plot matrix was used to find the relationship of LCC_{time} to LCC_{time+1} using Geoda software (https://spatial.uchicago.edu). Time was the year taken for temporal variation of Chlorophyll.

3. Results And Discussion

3.1. Performance of vegetation indices

3.1.1. Linear regression of LCC and sentinel derived vegetation indices

Leaf reflectance was used to derive the vegetation indices listed in Table 2. The spatial map of Sentinel derived vegetation indices is given in Fig. 5. At leaf-level, the relationships between the vegetation indices and LCC were computed. The narrowband vegetation indices with the most explanatory power ($R^2 > 0.7$) were Normalized difference vegetation index (45), and pigment specific simple ratio (Fig. 6). When coefficients of determination computed, vegetation indices pursued a similar pattern showing an expansion in the level of measured variation in LCC.

3.1.2. Chlorophyll Concentration and Landsat 8 vegetation indices

One Landsat 8 image acquired in November 2017 were used to derive broadband vegetation indices (Table2) for comparison with LCC derived from sentinel 2A. The spatial map of Landsat derived vegetation indices is given in Fig. 7. The average LCC plotted against its corresponding pixel on the Landsat 8 vegetation indices and the coefficient of determination was computed. The correlation analyses showed that Landsat 8 infrared percentage index is the broadband vegetation index was most sensitive to LCC (R^2 = 0. 8) (Fig. 8). The linear model was used that produced this large correlation, described by Eq. 7, to construct an LCC map.

$$y = -78.41 + 157.725 \times (1) \quad (7)$$

Where x = pixel value of the Landsat 8 infrared percentage index image. From the box transformation of this linear regression, found that the coefficient of determination improved from the simple regression, and R square reached 0.84.

3.2. Variations in chlorophyll Spatio-temporal

Landsat 8 OLI satellite image acquired in November 2017 because vegetation vigour was high in the month. Using Eq. (1), LCC was mapped for every pixel based on Landsat data. A similar method was applied to Landsat images obtained at various dates to map LCC (Fig. 9). Maps can show the spatial-temporal distribution of LCC. Larger LCC values were seen at the core of the forest, the higher amount of chlorophyll presented in the very dense part of the woods.

The area where a high amount of chlorophyll was found has protected by the forest (layer of trees acts as a boundary itself, as they are free from outer disturbance. The low amount of chlorophyll was present in edges of the forest because they were in proximity to external interference from non -forest activities.

Regarding the temporal variability, the maps depicted a decreasing gradient of LCC from November 1997 to November 2017 (Fig. 10). As far as anyone is concerned, this was the first occasion when that Landsat 8 used to outline LCC of sub-tropical timberland at the temporal scale.

3.3. Modelling Change detection

The LCC value was in decreasing trend from 1997 to 2017(rate = -1.2μgcm^{-2}year^{-1}) (Fig. 10). By the change analysis, overall, 33% of plants stress or forest health decline were predicted in the forest mainly because of pollution from crasher mine and other industrialization activities. The decreasing trend of variance from 1997 to 2017 showed large area of vegetation have low value of LCC in 2017 compared to 1992.

Scatter plot matrix of same variable from different base year is presented in Fig. 11, the base year was shown in x axis. From the regression analysis of two period taken from base year and independent variable (1997 to 2017), all shows significance changes (Fig. 11). The momentous changes occur between 1997 to 2017 having R^2 less than 0.6. Major changes occurred between the base year 2000 and independent variable 2013(R^2 = 0.60). Other change between base years and independent variable from 1997 to 2017 can be seen in the Fig. 11.

4. Discussion

The reason for infrared percentage index shows a strong relationship with LCC because the green edge acted like a red edge in the respect that both sides shift towards longer wavelengths at high LCC [43]. Therefore, in the study area, the low, dense forest having scrubs and grassland unable to show a good estimate of LCC. Thus, when LCC starts increasing, the green band becomes more sensitive, and the spectra of the red band become the lowest; that was the reason Landsat 8 infrared percentage index was best related to LCC. Although the LCC maps stood for a realistic spatiotemporal variation in LCC, many uncertainties were going with to them as it is constructed over assumptions and limitations. For estimating LCC of the forest the inversion of PROSAIL model was used. PROSAIL has been reversed over wide range of foliage canopies [43–50] with various levels of success. LAI is the prime part of measuring biophysical parameters in the forest [51–52]. Additionally, variation in leaf moisture, changes in soil moisture, changes in soil reflectance and differences in plant structure affect the linkage between Landsat 8 vegetation indices and LCC[29], particularly at LAI less than 3[53]. Although this suspicion requires further examination, there are motivations to accept that LAI does not change much temporally. It is likewise critical to take note that the low LCC values was affected by uncertainty. Other uncertainties in the accuracy of estimation in the years 2013 and 2017 arise because of sensor characteristics changes. The results used a new age of satellites rises above the abilities of the Landsat in terms of spatial resolution, swath width, number of spectral bands, and revisit time [54].

Forest become less productive with such decline of LCC (33%) from declining of gross primary productivity [55] and affects carbon uptakes with overall biogeochemical cycling. In the study area, as the canopy density [24] were declining gives rise to open forest. Open forest has combination of new and old tress, having varying height. In the 2017 and 2013 the LCC value was minimum. These minimum values showed increment of diseases in plants and corresponding stress would rise mortality of trees.

5. Conclusion

The result showed the relationship between vegetation indices and the biophysical parameters, showing which multispectral indices best explained the variation on LCC. The ability of broadband and narrowband vegetation indices was evaluated to predict forest LCC at different scales. Indices with spectral bands around the red edge (705–753 nm), pigment specific simple ratio and normalized difference index (45) indices were the most sensitive LCC ($R2 > 0.7$). A key finding was that the best performing Landsat 8 vegetation index was infrared percentage index, which explained 80% of the variation in LCC. The infrared percentage index better performed than NDVI for the retrieval LCC. Landsat satellite data retrieved vegetation indices was more sensitive to LCC than Sentinel derived vegetation indices.

The linear model portraying the connection between LCC used to delineate the Spatio-temporal variability of LCC in the forest scene. The examination exhibited that the medium-resolution and multispectral Landsat 8 used to measure LCC in tropical woodlands where ground systems and other potential devices were not applied, and the utilization of mapping procedures dependent on satellite information is essential. The LCC showed declining from 1997 to 2017 resembles forest health decline. The 33% of decreased of LCC in 2017 compared to 1997 revealed 33% increase in plant stress.

A practice use of this outcome was that future endeavours to determine LCC in a forest using multispectral remote sensing ought to consider the use of Landsat 8 infrared percentage index. The study likewise certified the importance of the red edge bands to anticipate LCC at the leaf level. Prescribed that future research should concentrate on testing existing and recently created algorithms to determine LCC in forest using the new age of satellites that beat the abilities of current sensors.

List Of Abbreviations

LCC: Leaf Chlorophyll Content

NDVI: Normalized Difference Vegetation Index

RMSE: Root-mean-square Deviation

NIR: Near Infrared

DN = Digital Number

Declarations

Ethical Approval and Consent to participate

The study received approval from the institutional review board of Central university of Jharkhand.

Consent for publication

The Author guarantees that the Contribution to the Work has not been previously published elsewhere.

Availability of supporting data

Not applicable

Competing interests

No competing interest

Funding

National fellowship for disabilities (NFD: 2015-2017-JHA-549)

Authors' contributions

First author has done the analysis and writing of manuscript. The second author has done editing activities.

Acknowledgements

We like to thank the forest department of Jharkhand (Van Bhawan, Doranda, Ranchi, Jharkhand, India) for its valuable contribution in the field visits. We like to thank USGS earth explorer for supplying Landsat data and ESA Copernicus for Sentinel 2A.

References

1. Allen CD, Macalady AK, Chenchouni H, Bachelet D, McDowell N, Vennetier M, Kitzberger T, Rigling A, Breshears DD, Hogg EHT, Gonzalez P, Fensham R, Zhang Z, Castro J, Demidova N, Lim JH, Allard G, Running SW, Semerci A, Cobb N (2010) A global overview of drought and heat-induced tree mortality reveals emerging climate change risks for forests. For. Ecol. Manage. 259:25. https://doi.org/10.1016/j.foreco.2009.09.001.
2. Macpherson MF, Kleczkowski A, Healey JR, Quine CP, Hanley N (2017) The effects of invasive pests and pathogens on strategies for forest diversification. Ecol. Model. 350:87–99. https://doi.org/10.1016/j.ecolmodel.2017.02.003.
3. Senf C, Seidl R, Hostert P (2017b) Remote sensing of forest insect disturbances: current state and future directions. Int. J. Appl. Earth Obs. Geoinform. 60:49–60. https://doi.org/10.1016/j.jag.2017.04.004.
4. Van LP, Lindquist E, Sathyapala S, Franceschini G (2015) Global forest area disturbance from fire, insect pests, diseases and severe weather events. For. Ecol. Manage. 352:78– 88. http://doi.org/10.1016/j.foreco.2015.06.010\.

5. Hilker T, Lyapustin AI, Tucker CJ, Hall FG, Myneni RB, Wang Y (2014) Vegetation dynamics and rainfall sensitivity of the Amazon. Proc. Natl. Acad. Sci. 111 (45):16041–16046. http://dx.doi.org/10.1073/pnas.1404870111.
6. Wu J, Albert LP, Lopes AP, Restrepo-Coupe N, Hayek M, Wiedemann KT (2016a) Leaf development and demography explain photosynthetic seasonality in Amazon evergreen forests. http://dx.doi.org/10.1126/science.aad5068.
7. Cox PM, Betts RA, Collins M, Harris PP, Huntingford C, Jones CD (2004)Amazonian forest dieback under climate-carbon cycle projections for the 21st century. Theoret. Appl. Climatol. 78 (1–3):137–156. http://dx.doi.org/10.1007/ s00704-004-0049-4.
8. Malhi Y, Roberts JT, Betts RA, Killeen TJ, Li W, Nobre CA (2008) Climate Change, Deforestation, and the Fate of the Amazon. http://dx.doi.org/10. 1126/science.1146961 (January 11).
9. Mendes De Moura Y, Soares Galvão L, Hilker, T, Wu J, Saleska S, Hummel Do Amaral C, Aragão EOC (2017) Spectral analysis of amazon canopy phenology during the dry season using a tower hyperspectral camera and modis observations. ISPRS Journal of Photogrammetry and Remote Sensing 131:52–64. https://doi.org/10.1016/j.isprsjprs.2017.07.006.
10. Richardson AD, Anderson RS, Arain MA, Barr AG, Bohrer G, Chen G (2012) Terrestrial biosphere models need better representation of vegetation phenology: results from the North American Carbon Program Site Synthesis. Glob. Change Biol. 18 (2): 566–584. http://dx.doi.org/10.1111/j.1365-2486.2011.02562.x.
11. Cleland EE, Chuine I, Menzel A, Mooney HA, Schwartz MD (2007) Shifting plant phenology in response to global change. Trends Ecol. Evol. 22 (7):357– 365. http://dx.doi.org/10.1016/j.tree.2007.04.003.
12. Richardson AD, Duigan SP, & Berlyn GP (2002) An evaluation of non-invasive methods to estimate foliar chlorophyll content. New phytologist 153(1):185-194.
13. Carter GA, Knapp AK (2001) Leaf optical properties in higher plants: Linking spectral characteristics to stress and chlorophyll concentration. Am. J. Bot. 88:677–684.
14. Peñuelas J, Filella I (1998) Visible and near-infrared reflectance techniques for diagnosing plant physiological status. Trends Plant. Sci. 3:151–156.
15. Yang H, Yang X, Heskel M, Sun S & Tang J (2017) Seasonal variations of leaf and canopy properties tracked by ground-based NDVI imagery in a temperate forest OPEN. Scientific Report 7(1267). https://doi.org/10.1038/s41598-017-01260-y.
16. Pastor-Guzman J, Atkinson P, Dash J & Rioja-Nieto R (2015) Spatiotemporal variation in mangrove chlorophyll concentration using Landsat 8. Remote sensing 7(11):14530-14558.
17. Zarco-Tejada PJ, Hornero A, Hernández-Clemente R & Beck PSA (2018) Understanding the temporal dimension of the red-edge spectral region for forest decline detection using high-resolution hyperspectral and Sentinel-2a imagery. ISPRS Journal of Photogrammetry and Remote Sensing 137:134–148. https://doi.org/10.1016/j.isprsjprs.2018.01.017.

18. Croft H, Chen JM & Zhang Y(2014) Temporal disparity in leaf chlorophyll content and leaf area index across a growing season in a temperate deciduous forest. International Journal of Applied Earth Observation and Geoinformation 33:312–320. https://doi.org/10.1016/j.jag.2014.06.005.
19. Goel NS (1988) Models of vegetation canopy reflectance and their use in estimation of biophysical parameters from reflectance data. Remote Sensing Reviews. https://doi.org/10.1080/02757258809532105.
20. Jacquemoud S, Bare F (1990) PROSPECT: a model of leaf optical properties spectra. Remote Sens Environ. 34:75–91.
21. Verhoef W(1984) Light scattering by leaf layers with application to canopy reflectance modelling: the SAIL model. Remote Sens Environ. 16:125–41.
22. Connelly XM (1997) The Use of a chlorophyll meter (SPAD-502) for field determinations of red mangrove (Rhizophora Mangle L.) leaf chlorophyll amount. NASA Univ. Res. Cent. Tech. Adv. Educ. Aeronaut. Space Auton. Earth Environ 1: 187–190.
23. Flores-de-Santiago F, Kovacs JM, Flores-Verdugo F (2013) Assessing the utility of a portable pocket Instrument for estimating seasonal mangrove leaf chlorophyll contents. Bull. Mar. Sci. 89:21–633.
24. Gupta SK & Chandra PA (2018) Forest Canopy Density and Fragmentation Analysis for Evaluating Spatio-Temporal Status of Forest in the Hazaribagh Wild Life Sanctuary, Jharkhand (India). Research Journal of Environmental Sciences 12(4):198–212.https://doi.org/10.3923/rjes.2018.198.212.
25. Gupta SK & Pandey AC (2019) Change detection of landscape connectivity Change detection of landscape connectivity arisen by forest transformation in Hazaribagh wildlife sanctuary, Jharkhand 5 (India). Spatial Information Research. https://doi.org/10.1007/s41324-019-00301-0
26. Kumari B and Pandey AC (2019) MODIS based forest fire hotspot analysis and its relationship with climatic variables. Spatial Information Research. http://doi.org/10.1007/s41324-019-00275-z.
27. CHAVEZ PS (1989) Radiometric calibration of Landsat thematic mapper multispectral images. Photogrammetric Engineering and Remote Sensing 55:1285–1294.
28. Sehgal VK, Chakraborty D & Sahoo RN (2016) Inversion of radiative transfer model for retrieval of wheat biophysical parameters from broadband reflectance measurements. Information Processing in Agriculture 3(2):107–118. https://doi.org/10.1016/j.inpa.2016.04.001
29. Blackburn GA (2007) Hyperspectral remote sensing of plant pigments. J. Exp. Bot. 58:855–867.
30. Crippen R (1990) Calculating the Vegetation Index Faster. Remote Sensing of Environment 34: 71-73
31. Kauth R and Thomas G (1976) The Tasselled Cap-A Graphic Description of the Spectral-Temporal Development of Agricultural Crops as Seen by Landsat. In Proceedings of the LARS Symposium of Machine Processing of Remotely-Sensed Data, West Lafayette, IN: Purdue University, pp. 4B41-4B51.
32. Pinty B & Verstraete MM (1992) GEMI: a non-linear index to monitor global vegetation from satellites. Vegetation 101(1):15-20.
33. Gitelson AA, Kaufman YJ & Merzlyak MN (1996) Use of a green channel in remote sensing of global vegetation from EOS-MODIS. Remote sensing of Environment 58(3):289-298

34. Tucker C (1979) Red and Photographic Infrared Linear Combinations for Monitoring Vegetation. Remote Sensing of Environment 8:127–150.
35. Kaufman YJ & Tanre D (1992) Atmospherically resistant vegetation index (ARVI) for EOS-MODIS. IEEE transactions on Geoscience and Remote Sensing 30(2): 261-270.
36. Birth GS and McVey G(1968) Measuring the color of growing turf with a reflectance spectroradiometer. Agronomy Journal 60:640-643.
37. Blackburn GA (1998) Spectral indices for estimating photosynthetic pigment concentrations: a test using senescent tree leaves. Int. J. Remote Sens. 19:657-675
38. Delegido J, Verrelst J, Alonso L, Moreno J (2011) Evaluation of sentinel-2 red-edge bands for empirical estimation of green LAI and chlorophyll content. Sensors 11(7):7063-708.
39. Asner GP & Martin RE(2008) Spectral and chemical analysis of tropical forests: Scaling from leaf to canopy levels. Remote Sensing of Environment 112(10): 3958-3970.
40. Glenn E, Huete A, Nagler P, Nelson S (2008) Relationship between remotely-sensed vegetation indices, canopy attributes and plant physiological processes: What vegetation indices can and cannot tell us about the landscape. Sensors 8(4): 2136-2160.
41. Buermann W, Wang Y, Dong J, Zhou L, Zeng X, Dickinson RE & Myneni RB (2002) Analysis of a multiyear global vegetation leaf area index data set. Journal of Geophysical Research: Atmospheres 107(D22): ACL-14.
42. Chen W, Cao C (2012) Topographic correction-based retrieval of leaf area index in mountain areas. Journal of Mountain Science 9(2):166-174.
43. Gitelson AA(2005) Remote estimation of canopy chlorophyll content in crops. Geophys. Res. Lett. 32. doi:10.1029/2005GL022688
44. Darvishzadeh R, Atzberger C, Skidmore AK, Abkar AA (2009) Leaf area index derivation from hyperspectral vegetation indices and the red edge position. Int.J. Remote Sens. 30: 6199–6218, http://dx.doi.org/10.1080/01431160902842342
45. Jacquemoud S, Baret F, Andrieu B, Danson FM, Jaggard K (1995) Extraction of vegetation biophysical parameters by inversion of the PROSPECT + SAIL models on sugar beet canopy reflectance data. Application to TM and AVIRIS sensors. Remote Sens. Environ. 52:163–172. http://dx.doi.org/10.1016/0034-4257(95)00018-
46. Le Maire G, Marsden C, Verhoef W, Ponzoni FJ, Lo Seen D, Bégué A, Stape JL, Nouvellon Y (2011) Leaf area index estimation with MODIS reflectance time series and model inversion during full rotations of Eucalyptus plantations. Remote Sens. Environ. 115: 586–599.http://dx.doi.org/10.1016/j.rse.2010.10.004
47. Meroni M, Colombo R, Panigada C (2004) Inversion of a radiative transfer model with hyperspectral observations for LAI mapping in poplar plantations. Remote Sens. Environ. 92:195–206. http://dx.doi.org/10.1016/j.rse.2004.06.005.
48. Richter R, Schläpfer D, Müller A (2011) Operational atmospheric correction for imaging spectrometers accounting for the smile effect. IEEE Trans. Geosci. Remote Sens. 49: 1772–1780.

http://dx.doi.org/10.1109/TGRS2010.2089799.

49. Si Y, Schlerf M, Zurita-Milla R, Skidmore A, Wang T (2012) Mapping spatio-temporal variation of grassland quantity and quality using MERIS data and the PROSAIL model. Remote Sens. Environ. 121:415–425.http://dx.doi.org/10.1016/j.rse.2012.02.011
50. Richter K, Atzberger C, Vuolo F, Weihs P, D'Urso G (2009) Experimental assessment of the sentinel-2 band setting for RTM-based LAI retrieval of sugar beet and maize. Can. J. Remote Sens. 35:230–247. http://dx.doi.org/10.5589/m09-010.
51. Roberts DA, Ustin SL, Ogunjemiyo S, Greenberg J, Dobrowski SZ, Chen J, Hinckley TM(2004) Spectral and structural measures of northwest forest vegetation at leaf to landscape scales. Ecosystems 7:545–562.
52. Green EP, Edwards AJ(2000) Remote Sensing Handbook for Tropical Coastal Management, UNESCO Publisher: Paris, France.
53. Díaz BM, Blackburn GA(2003) Remote sensing of mangrove biophysical properties: Evidence from a laboratory simulation of the possible effects of background variation on spectral vegetation indices. Int. J. Remote Sens. 24:53–73.
54. Drusch M, Del Bello U, Carlier S, Colin O, Fernandez V, Gascon F, Hoersch B, Isola C, Laberinti P, Martimort P (2012) Sentinel-2: ESA's optical high-resolution mission for GMES operational services. Remote Sens. Environ. 120:25–36.
55. Li Y, He N, Hou J, Xu L, Liu C, Zhang J, Wang Q, Zhang X, Wu X (2018) Factors influencing leaf chlorophyll content in natural forests at the biome scale. Frontiers in Ecology and Evolution.

Figures

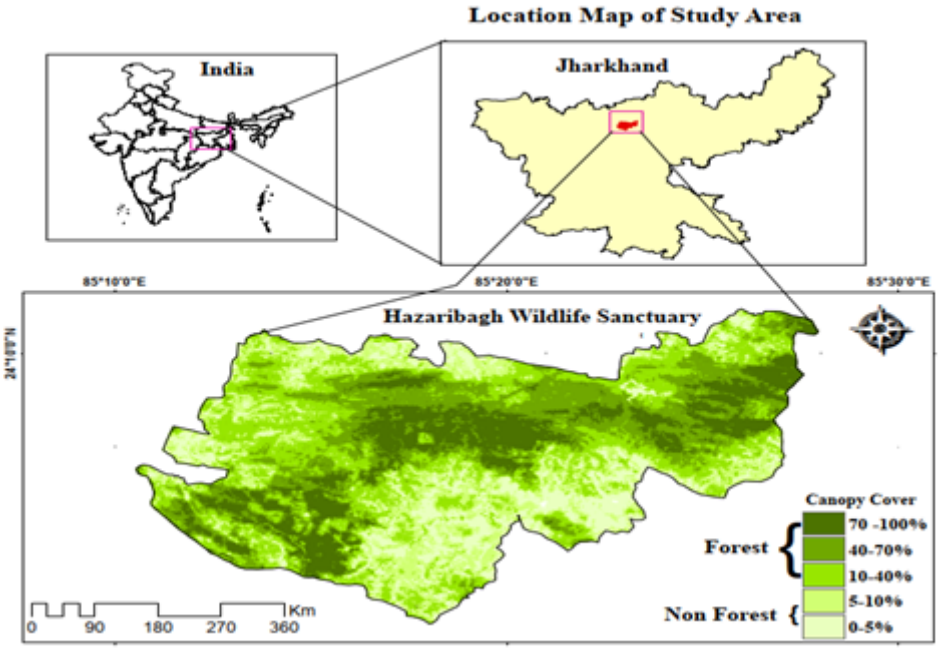

Figure 1

Study Area: Hazaribagh Wildlife Sanctuary

Figure 2

Transformation of forest cover into open forest and scrub

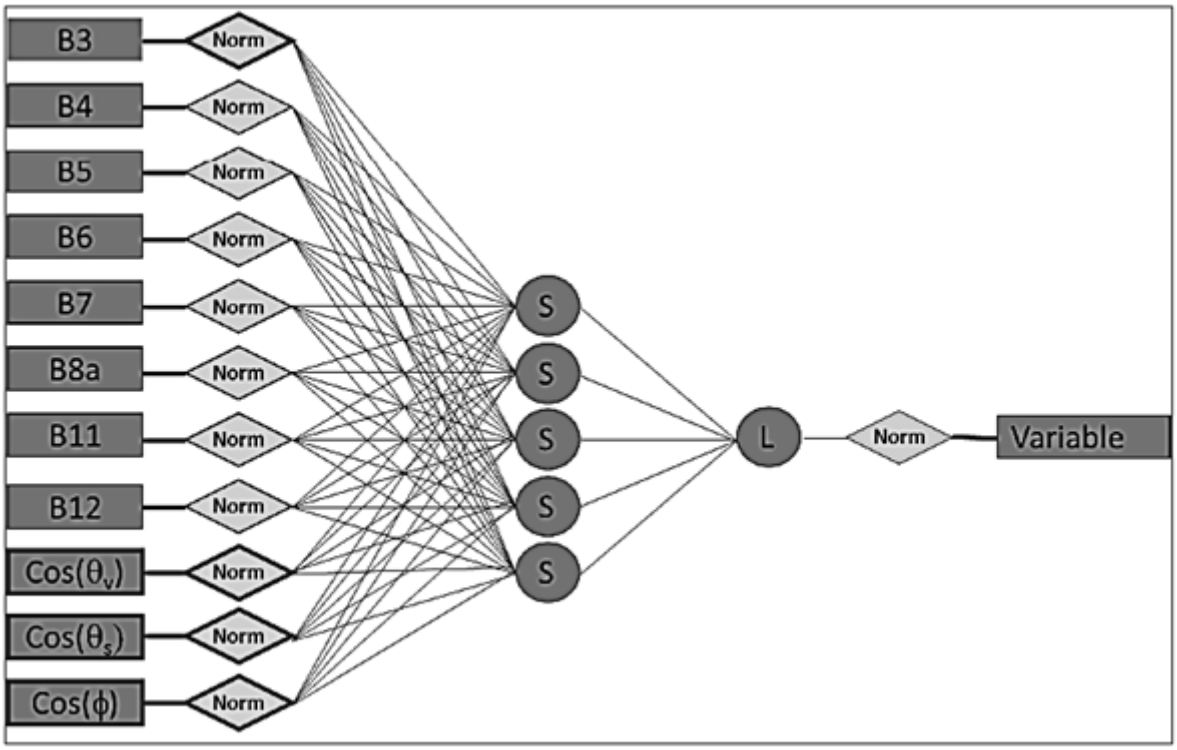

Figure 3

Neural network structures based invertion of radiative transfer model(PROSAIL) designed for assessment of the biophysical variables considered from the 8 SENTINEL2 bands and the 3 that define the geometry of observation. The network is constructed over 1 linear output neuron and 1 hidden level of 5 neurons . The ‘Norm’ symbols indicating to the normalization process. Symbols ‘S’ and ‘L’ conform sigmoid (tansig) and linear transfer functions of the neurons respectively.

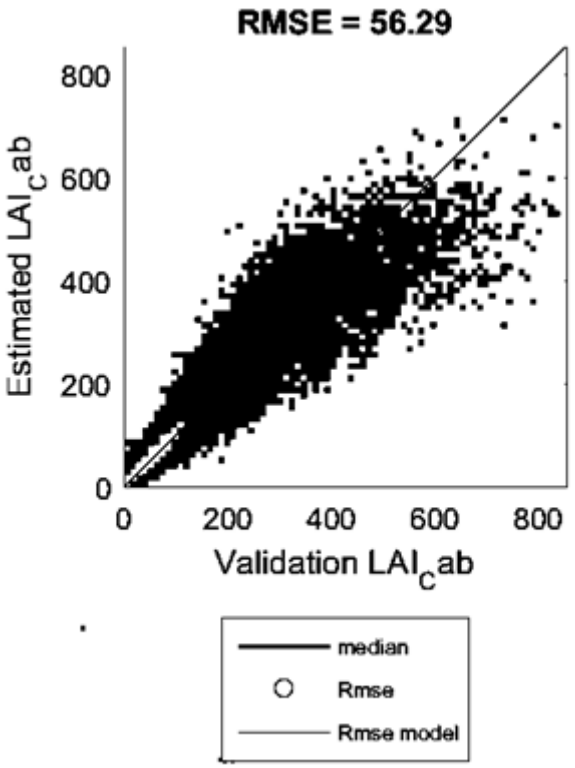

Figure 4

Performances of the neural networks for Leaf Chlorophyll Content (LAI Cab) on the test database (Source: http://step.esa.int/docs/extra/ATBD_S2ToolBox_L2B_V1.1.pdf)

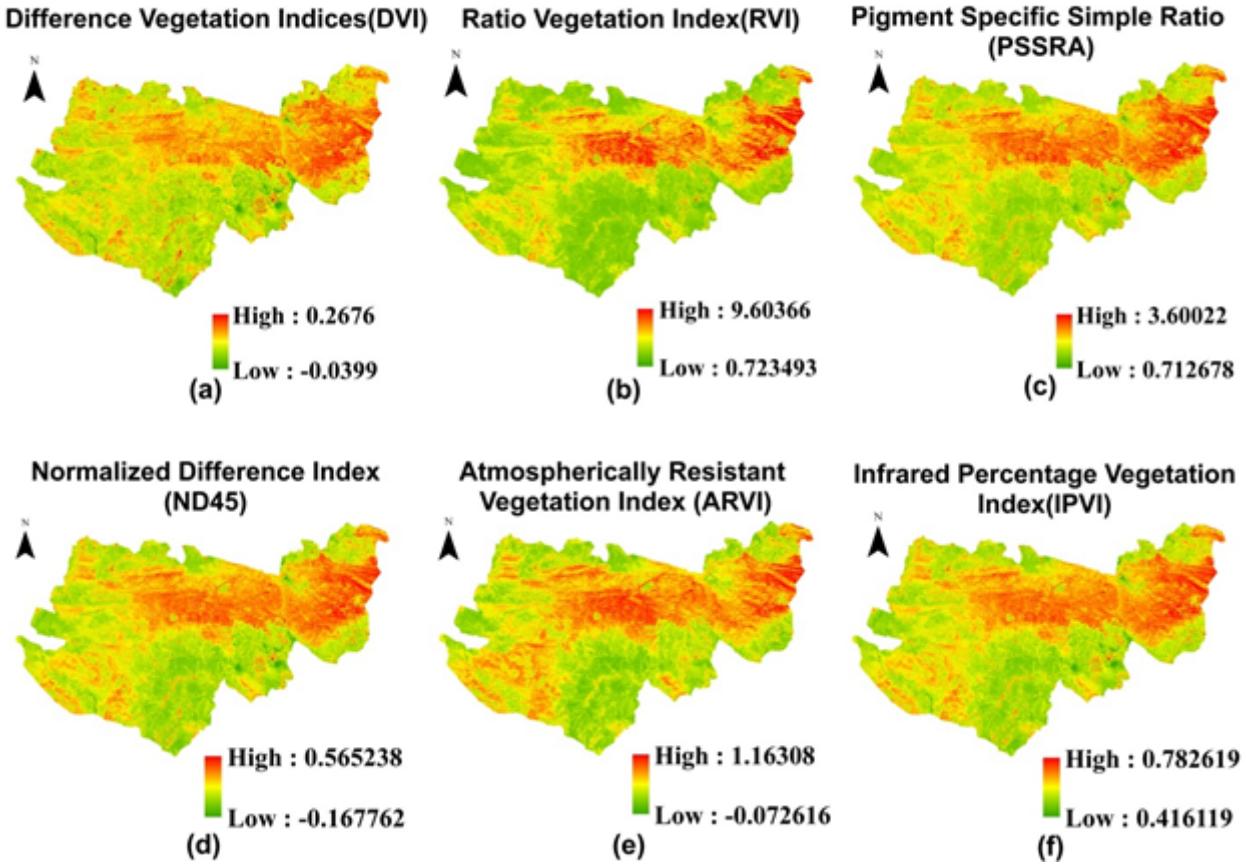

Figure 5

Sentinel 2A derived vegetation Indices

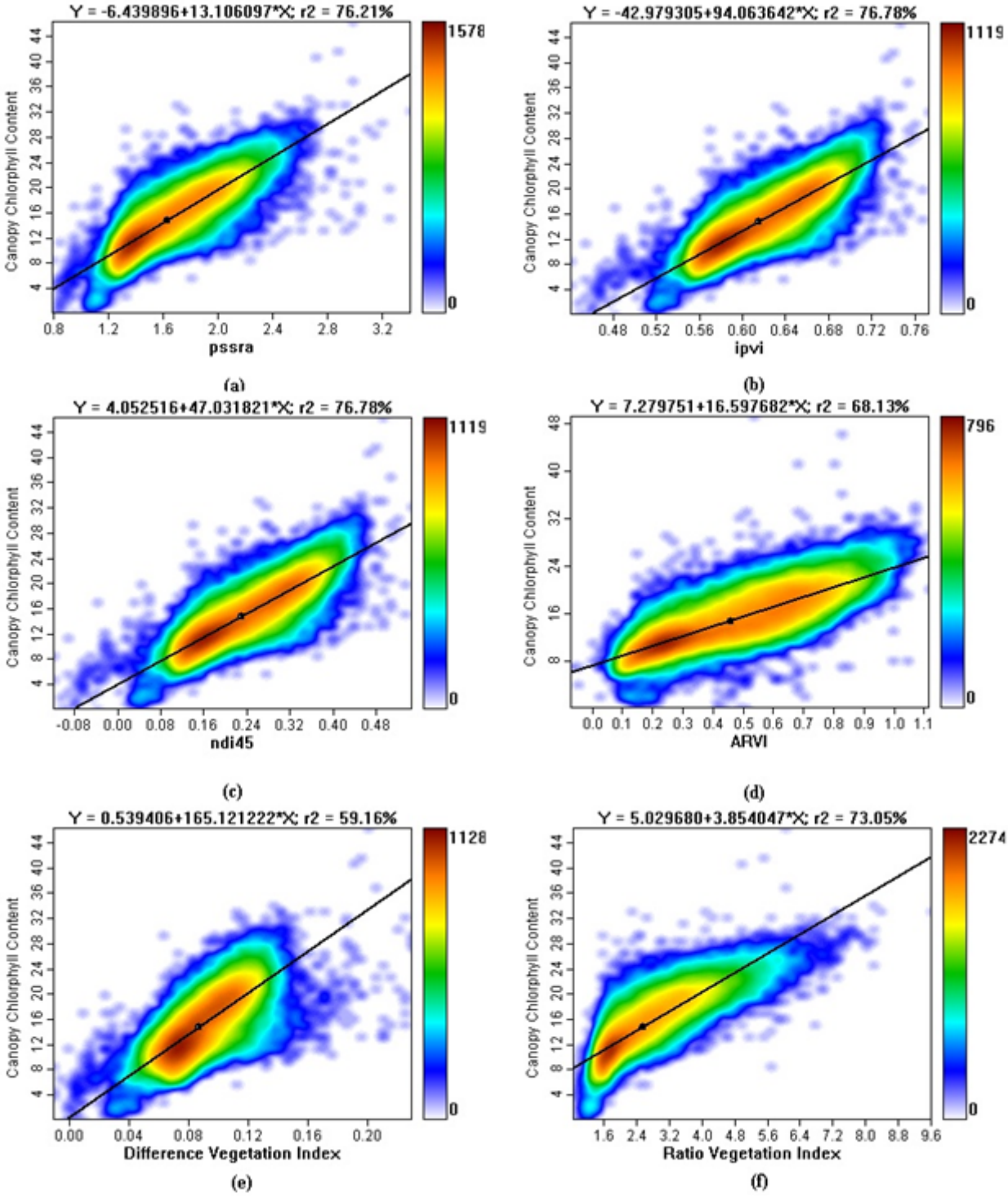

Figure 6

Sensitivity analysis of sentinel derived vegetation indices with chlorophyll content(µgcm-2)

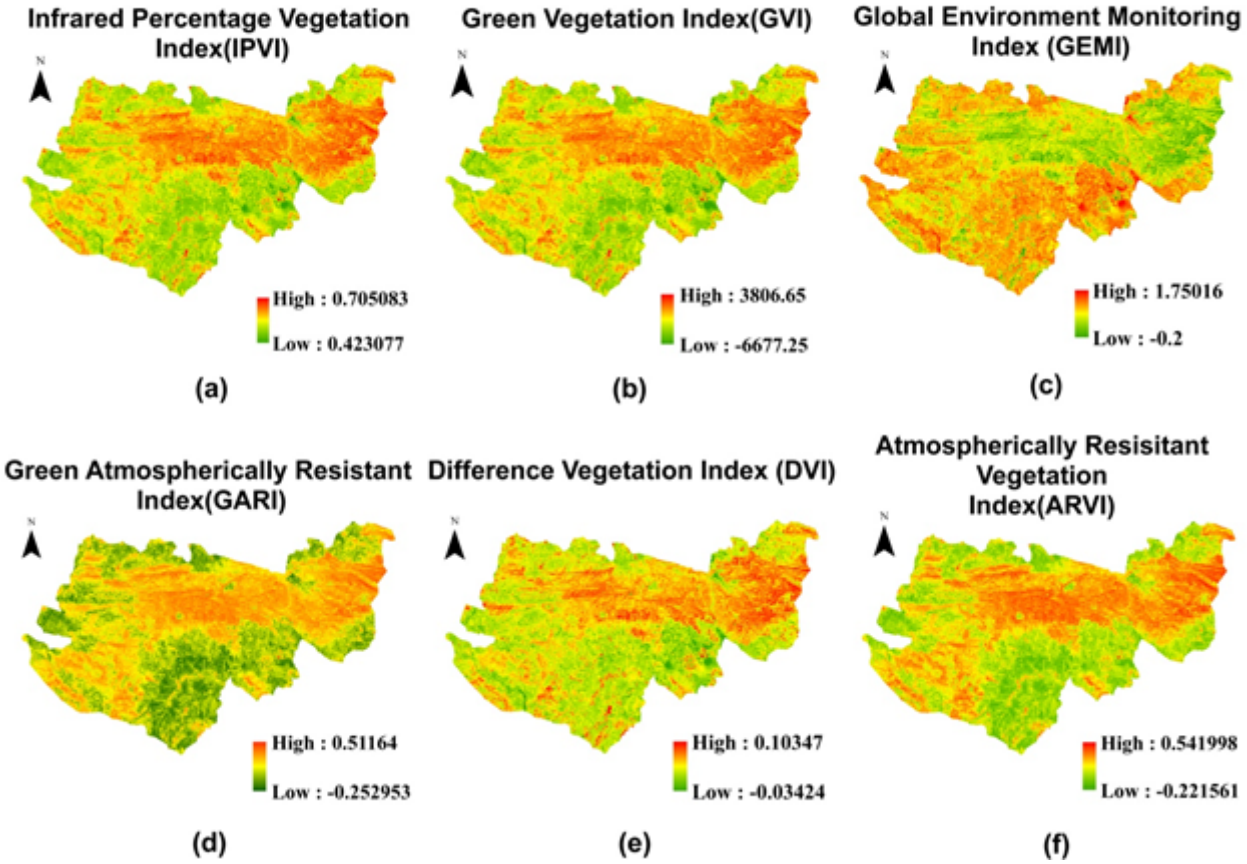

Figure 7

Spectral vegetation indices (Landsat) used in the study

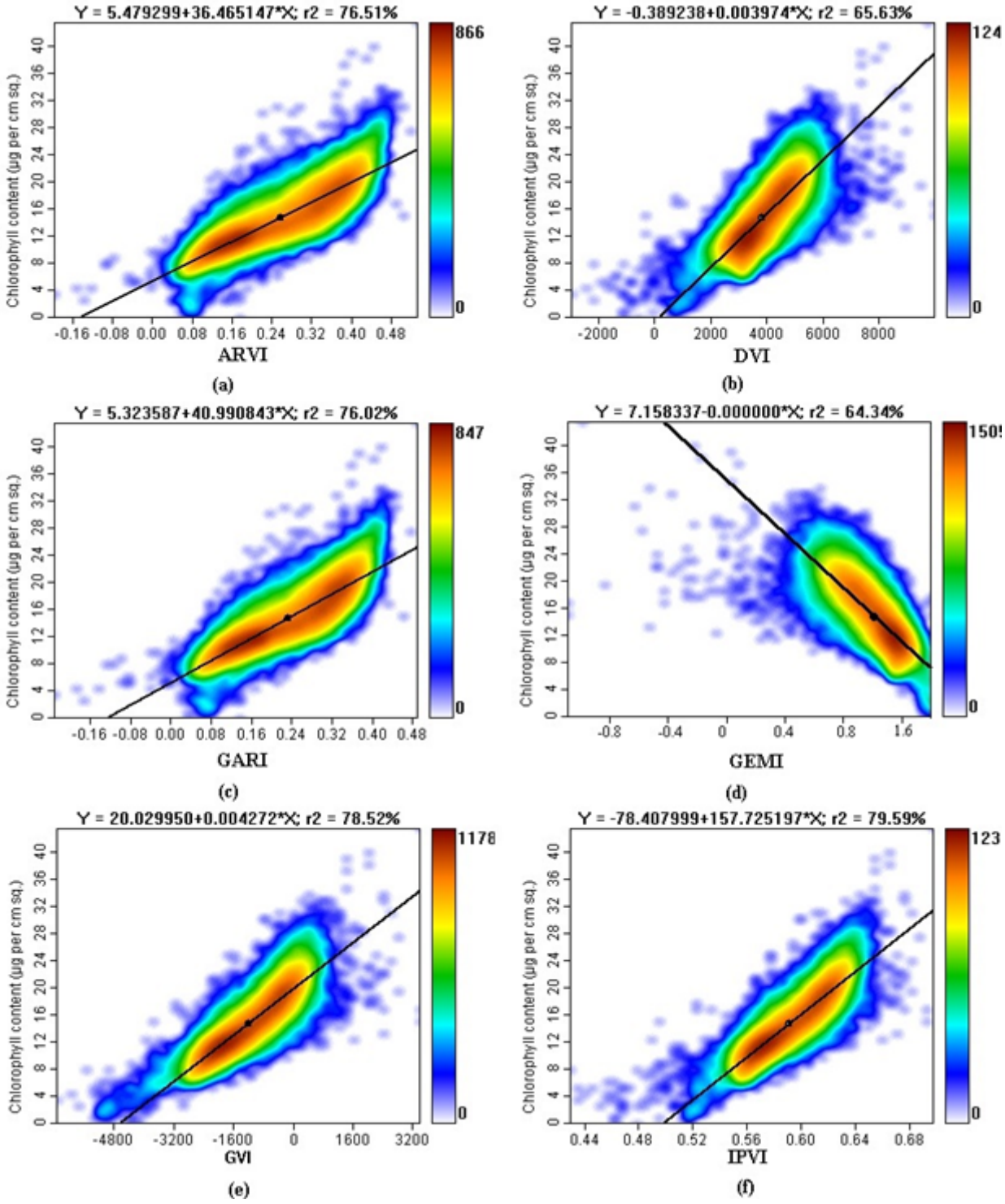

Figure 8

Sensitivity analysis of vegetation Indices (Landsat) with chlorophyll Content(µgcm-2)

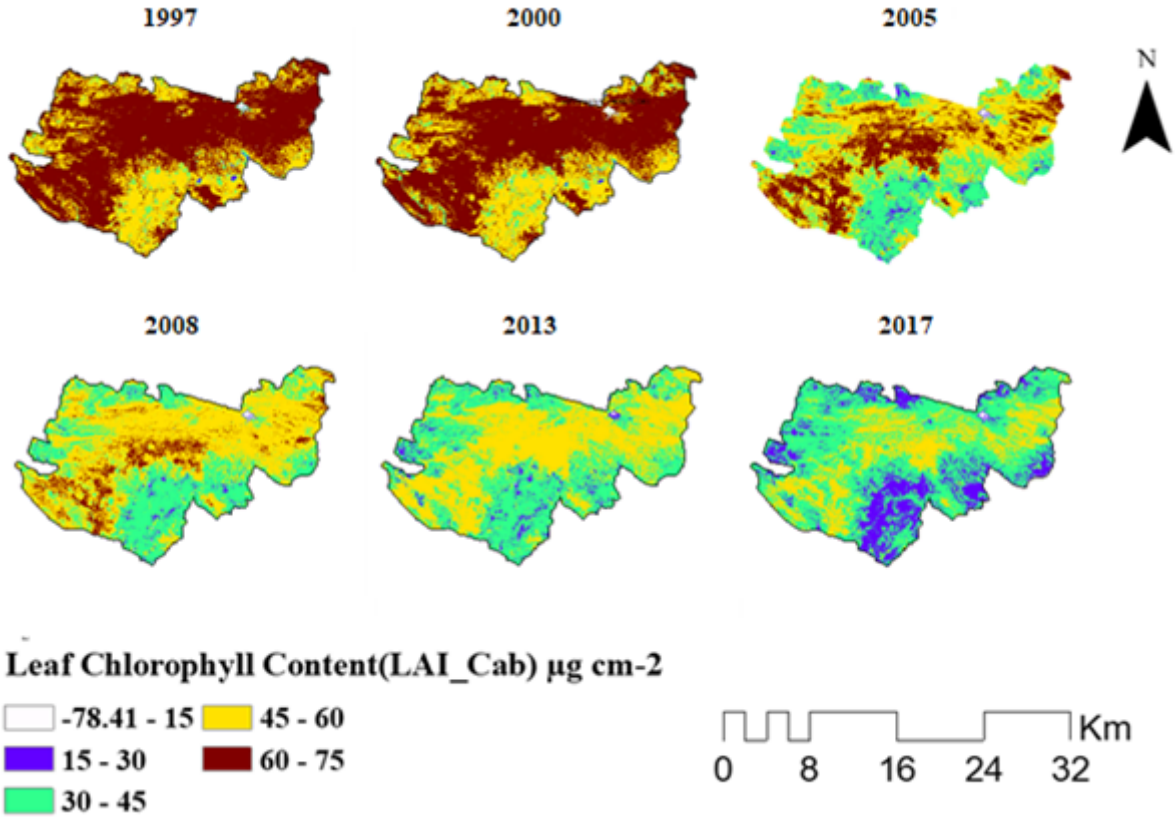

Figure 9

Spatio-Temporal variation of LCC or lAI_Cab ((1997 to 2017)

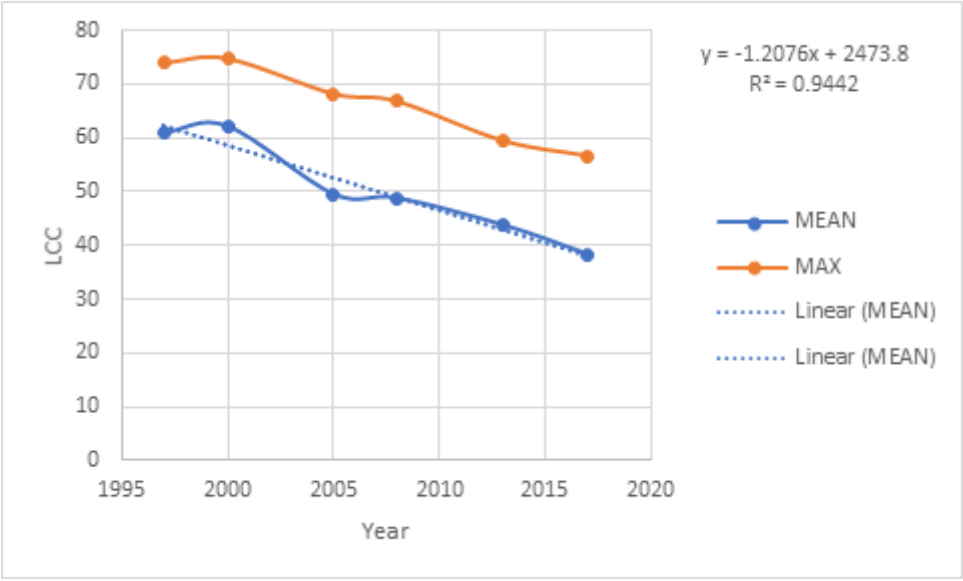

Figure 10

Statistics of Spatio- temporal variation of LCC

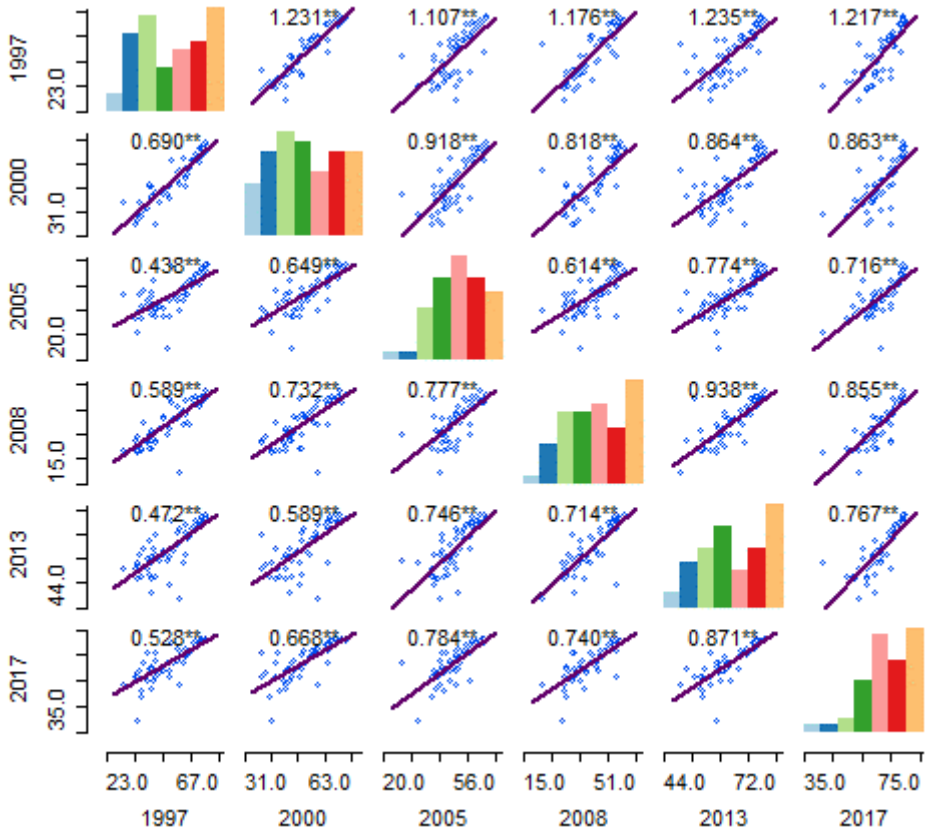

Figure 11

Time series regression of LCC from 1997 to 2017

Supplementary Files

This is a list of supplementary files associated with this preprint. Click to download.

- Equation1.jpg